Structure and three-body decay of ^{9}Be resonances

R. Álvarez-Rodríguez,[1,2,*] A. S. Jensen,[1] E. Garrido,[3] and D. V. Fedorov[1]
[1]*Department of Physics and Astronomy, University of Aarhus, DK-8000 Aarhus C, Denmark*
[2]*Grupo de Física Nuclear, Departamento de Física Atómica, Molecular y Nuclear, Universidad Complutense de Madrid, E-28040 Madrid, Spain*
[3]*Instituto de Estructura de la Materia, Consejo Superior de Investigaciones Científicas, Serrano 123, E-28006 Madrid, Spain*
(Received 6 July 2010; published 9 September 2010)

The complex-rotated hyperspherical adiabatic method is used to study the decay of low-lying ^{9}Be resonances into one neutron and two α particles. We investigate the six resonances above the breakup threshold and below 6 MeV: $1/2^{\pm}$, $3/2^{\pm}$, and $5/2^{\pm}$. The short-distance properties of each resonance are studied, and the different angular momentum and parity configurations of the ^{8}Be and ^{5}He two-body substructures are determined. We compute the branching ratio for sequential decay via the ^{8}Be ground state, which qualitatively is consistent with measurements. We extract the momentum distributions after decay directly into the three-body continuum from the large-distance asymptotic structures. The kinematically complete results are presented as Dalitz plots as well as projections on given neutron and α energy. The distributions are discussed and, in most cases, found to agree with available experimental data.

DOI: 10.1103/PhysRevC.82.034001 PACS number(s): 21.45.−v, 21.60.Jz, 25.70.Ef, 27.20.+n

I. INTRODUCTION

The structure of ^{9}Be has been extensively studied, both theoretically [1–16] and experimentally [17–27], but there are still large uncertainties in the structure and decay of the low-lying excited states. This is surprising and worrisome in view of the great effort and the expected rather accurate approximation as a simple three-body system where the intrinsic degrees of freedom are inactive. Are the problems related to inaccuracies of the theoretical models, the numerical techniques, direct experimental uncertainties, data analysis, or interpretation of the data in comparison with model results?

In theory, the three-body continuum problem is better handled and more accurately solved for nuclear systems with the special mixture of short- and long-range interactions. Observables rather close to the directly measured quantities can be delivered. In experiments, both beam quality detector systems and systematic analyses have improved substantially in recent years. This means that genuine three-body systems can be treated fully and precisely in both theory and experiment, more specifically complete kinematics of the fragments are available. The road to detailed comparison is, therefore, paved. The simplest systems should then be understood before reliability can be expected for more complicated scenarios.

Furthermore, the results of requested applications in astrophysics, where often the energies are too low to be reached experimentally, can only be indirectly tested by their implications. The approximations employed so far in predictions should then be tested by comparison. A reasonable procedure is to select a three-body system, compute and measure the best we can, and compare as detailed as possible. The choice of ^{9}Be is tempting as a rather simple system, which is accessible to both theory and experiments. In addition, this is a system of particular interest in astrophysics, where formation of ^{9}Be can proceed through the reaction $\alpha(\alpha n,\gamma)^9$Be. The subsequent reactions ^{9}Be$(\alpha,n)^{12}$C link to heavier elements in stellar nuclear synthesis responsible for the present Universe.

From the early days of nuclear physics, the structure of the ^{9}Be nucleus has been considered a prototype of the clusterlike structure of nuclei. Therefore, different types of three-body descriptions have been used to describe it: early cluster models [1–3,6,8], and more sophisticated ones (e.g., the resonating group model [7]), antisymmetrized molecular dynamics [10], or the microscopic multicluster model [14]. Moreover, many-body types of calculations have also been performed on ^{9}Be: projected Hartree-Fock [5], shell model [4], quantum Monte Carlo [12], and *ab initio* no-core shell model [15]. All of them are able to reproduce the low-lying energy spectrum and electromagnetic properties in fair agreement with the experimental data available at the moment, although, in general, theoretical models predict more states than are seen experimentally.

Somewhat surprisingly, the three-body decays of the ^{9}Be resonances have barely been studied [13,28]. The inverse process may proceed through the resonances, but nonresonant contributions are also important. Before facing this more complicated process, it is advisable to get a good understanding of the resonance decay of ^{9}Be into $\alpha\alpha n$. The experimentally known ^{9}Be states are shown in Fig. 1 for excitation energies below 6 MeV where all other particle thresholds other than $\alpha\alpha n$ are closed. All these levels, apart from $\frac{5}{2}^-$, have a fairly large width, which makes it difficult to determine their properties. Many experimental efforts have been addressed toward this $\frac{5}{2}^-$ state [17,19,22,26]. They all agree in the small percentage of the decay, which takes place via the ^{8}Be ground state. So far, no agreement has been reached with regard to its main decay path, via ^{8}Be(2^+), ^{5}He(p), or direct. Much less is known about the decays of other low-lying resonances of ^{9}Be. Both the $\frac{1}{2}^-$ and $\frac{5}{2}^+$ seem to prefer to decay through ^{8}Be(0^+), although especially, the results for $\frac{1}{2}^-$ need to be better established.

*raquel.alvarez@fis.ucm.es

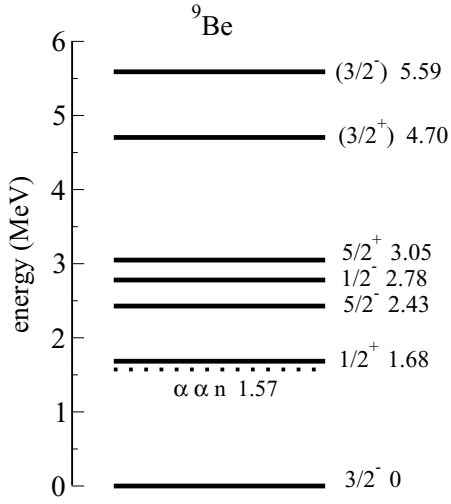

FIG. 1. Scheme of the experimentally known levels of ^{9}Be below 6 MeV of excitation energy.

The purpose of the present paper is to report on comprehensive calculations of the three-body properties of low-lying states in ^{9}Be. We give a survey of the short-distance structure of the resonances, their dynamic evolution across intermediate distances, which often is referred to as decay mechanism, and eventually, which reach the large-distance asymptotics, which reveal the complete set of momentum distributions of the fragments after decay. The two-dimensional energy correlations shown in Dalitz plots can be directly compared to the experimental data. This is the only information, which relates measurements with initial short-distance structure and decay mechanism. Extrapolations backward from data, therefore, necessarily must be model dependent. We attempt to provide an interpretation, which is as physically meaningful as possible.

II. THEORETICAL INGREDIENTS

The decay of ^{9}Be into two α particles and one neutron is obviously a three-body problem in the final state where the particles are far from each other. Furthermore, the dominant structure at small distances is also of cluster nature for these low-lying resonances. The Hamiltonian for this cluster structure is then

$$H = \sum_{i=}^{3} \frac{\boldsymbol{p}_i^2}{2m_i} - \frac{\boldsymbol{P}_t^2}{2M} + \sum_{i=1}^{3} V_i(\boldsymbol{r}_j - \boldsymbol{r}_k) + V_{3b}, \tag{1}$$

where $\boldsymbol{p}_i$ and m_i are the momentum and the mass of particle i, $\boldsymbol{P}_t$ is the total momentum, and V_i is the interaction between particles j and k. Here, $\{i, j, k\}$ is a cyclic permutation of $\{1, 2, 3\}$, and V_{3b} is a three-body potential, which depends on all three particle coordinates. It is convenient to substitute the position coordinates by the Jacobi coordinates $\boldsymbol{x}$ and $\boldsymbol{y}$ defined as

$$\begin{aligned} \boldsymbol{x} &= \sqrt{\frac{\mu_{12}}{m}}(\boldsymbol{r}_1 - \boldsymbol{r}_2), \\ \boldsymbol{y} &= \sqrt{\frac{\mu_{12,3}}{m}}\left(\boldsymbol{r}_3 - \frac{m_1\boldsymbol{r}_1 + m_2\boldsymbol{r}_2}{m_1 + m_2}\right), \end{aligned} \tag{2}$$

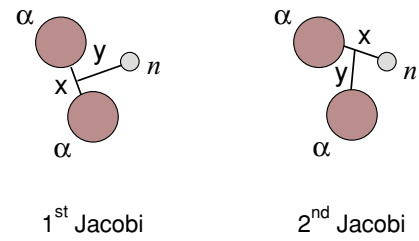

FIG. 2. (Color online) Scheme of the different Jacobi coordinates for ^{9}Be.

where m is an arbitrary mass scale chosen as the nucleon mass, and μ_{12} and $\mu_{12,3}$ are the reduced masses. The Hamiltonian becomes

$$H = -\frac{\hbar^2}{2m}\left(\nabla_x^2 + \nabla_y^2\right) + \sum_{i=1}^{3} V_i(\boldsymbol{x}, \boldsymbol{y}) + V_{3b}. \tag{3}$$

In the present case, we have two possible choices for Jacobi coordinates (see Fig. 2), which lead to different sets of $(\boldsymbol{x}, \boldsymbol{y})$ coordinates. We use hyperspherical coordinates where the six coordinates are $\{\rho,\alpha,\theta_x,\phi_x,\theta_y,\phi_y\}$. The θ's and ϕ's refer to the directions of $\boldsymbol{x}$ and $\boldsymbol{y}$, while $\alpha = \arctan(x/y)$ and $\rho = (x^2 + y^2)^{1/2}$ are related to their sizes. Actually, ρ is the only length coordinate, which describes the average distance from the center of mass.

Resonances are computed within the formalism of complex scaling of the hyperspherical coordinates. This is particularly simple, since only one coordinate, the hyper-radius ρ, has to be scaled. The Hamiltonian is complex rotated, that is,

$$H_\theta(\rho) = H(\rho e^{i\theta}). \tag{4}$$

We use the adiabatic expansion method and solve the Faddeev equations stepwise, that is, first the angular, then the (hyper) radial part [29]. The angular part of the Hamiltonian is first solved by keeping the value of ρ fixed, that is,

$$T_\Omega \Phi_{nJM}^{(i)} + \frac{2m}{\hbar^2}\rho^2 V_i \Phi_{nJM} = \lambda_n \Phi_{nJM}^{(i)}, \quad i = 1, 2, 3, \tag{5}$$

where n labels the adiabatic components. T_Ω is the angular part of the kinetic-energy operator [29]. This provides a complete set of angular wave functions Φ_{nJM} that are employed to expand the total wave function Ψ^{JM},

$$\Psi^{JM} = \frac{1}{\rho^{5/2}} \sum_n f_n(\rho)\Phi_{nJM}(\rho, \Omega), \tag{6}$$

where the ρ-dependent expansion coefficients $f_n(\rho)$ are the hyper-radial wave functions obtained from the coupled set of hyper-radial equations [29],

$$\begin{aligned} &\left\{-\frac{d^2}{d\rho^2} + \frac{2m}{\hbar^2}\left[V_{\text{eff}}^{(n)}(\rho) + V_{3b}(\rho) - E\right]\right\} f_n(\rho) \\ &\quad - \sum_{n'} \left(2P_{nn'}\frac{d}{d\rho} + Q_{nn'}\right) f_{n'}(\rho) = 0, \end{aligned} \tag{7}$$

where V_{3b} is a three-body potential used for fine-tuning and the functions $P_{nn'}$ and $Q_{nn'}$ are given, for instance, in Ref. [29]. The eigenvalues λ_n in Eq. (5) enter in Eq. (7) as a part of the

effective adiabatic potentials:

$$V_{\rm eff}^{(n)}(\rho) = \frac{\hbar^2}{2m}\frac{1}{\rho^2}\left[\lambda_n(\rho) + \frac{15}{4}\right]. \quad (8)$$

Resonances are usually understood as states with complex energy $E = E_R - i\Gamma_R/2$, where E_R is the energy of the resonance and Γ_R is the width. Now, if we define $k = \sqrt{2\mu|E|/\hbar^2}$, with μ as the reduced mass of the system, we then have that the asymptotic form of the resonance wave function is given by

$$f_n(\rho \to \infty) \sim e^{ik\rho\cos\beta}e^{k\rho\sin\beta}, \quad (9)$$

where $\beta = \frac{1}{2}\arctan(\frac{\Gamma_R}{2E_R})$. The first term oscillates, while the second one diverges. After the complex scaling transformation ($\rho \to \rho e^{i\theta}$), the radial asymptotic behavior becomes

$$f_n(\rho \to \infty) \sim e^{ik\rho\cos(\theta-\beta)}e^{-k\rho\sin(\theta-\beta)}, \quad (10)$$

which implies that when $\theta > \beta$, the wave function goes to zero exponentially and the resonance can then be obtained as an ordinary bound state. True bound states remain unchanged under the coordinate rotation.

For our particular case of ^{9}Be, the two-body interactions V_i are chosen to reproduce the low-energy scattering properties of the two different pairs of particles in our three-body system. We use the Ali-Bodmer α-α potential [30] supplemented by the Coulomb potential between α particles, and the α-neutron interaction is taken from Ref. [31]. The ^{9}Be resonances are of three-body character at large distances, since no other channels are open for these energies. This is not necessarily correct at short distances, where all nine nucleons (and their intrinsic structure) may contribute in different (cluster) configurations.

We use the (complex-scaled) three-body model at all distances because the decay properties only require the proper description of the emerging three particles. Therefore, the angular eigenfunctions and eigenvalues in Eq. (5) are complex, as well as all the terms entering in the coupled set of radial equations of Eq. (7). The missing information, if any, beyond the three-body structure, is the initial structure at small distances. This piece, which acts as a boundary condition, is parametrized through a short-range three-body potential of the form $V_{3b} = S\,\exp(-\rho^2/b^2)$.

Also, different three-body resonances correspond, in general, to different three-body structures. As a consequence, the missing information, which goes beyond the two-body correlations is, in principle, resonance dependent. Therefore, the strength (and possibly the range) in the three-body force is adjusted individually to give the correct position of each of the resonance energies. This adjustment implies that the potential is angular momentum dependent but this is already a property of the two-body potential. The corresponding Hamiltonian for the three-body problem still exists as a nonlocal operator, but this feature is already present due to the angular momentum dependence of the two-body interactions. Then, it is clear that this phenomenological fine-tuning does not arise from the presence of a genuine three-body interaction.

The energy dependence is all decisive for decay properties as evident in the exponential dependence of probability for tunneling through a barrier. On the other hand, the three-body potential is assumed to be completely structure independent, and, therefore, only marginally influences the partition between different structures at large distances. However, this is an assumption, which may be violated through the dynamic evolution from inaccurate initial small-distance boundary conditions provided by the three-body potential.

III. SHORT-DISTANCE STRUCTURE

The short-distance structures are crucial for the energies, whereas dominating configurations at large distances are decisive for the observable decay properties. The connection between these two regimes contains information about the decay mechanism, which, therefore, only is an observable effect precisely to the extent reflected in the final distributions. In other words, sensible theoretical models are indispensable to interpret the experimental results. In this section, we extract and discuss short-distance bulk properties, that is, effective potentials, energies, and partial-wave structure.

A. Adiabatic potentials and energies

Each of the adiabatic potentials entered in Eq. (7) corresponds to a specific combination of quantum numbers (i.e., partial-wave angular momenta between the particles in the different Jacobi systems). Usually, only rather few adiabatic potentials are needed to achieve convergence. In Fig. 3, we show the real part of these adiabatic potentials as defined in Eq. (8) plus the three-body potential individually fitted for each spin and parity to reproduce the experimental resonance energies. We did not include the nonadiabatic diagonal parts in the figure [Q_{nn} in Eq. (7), $P_{nn} = 0$] because they usually are insignificant and, in a sense, more related to the coupling between the different radial potentials. The only exception is

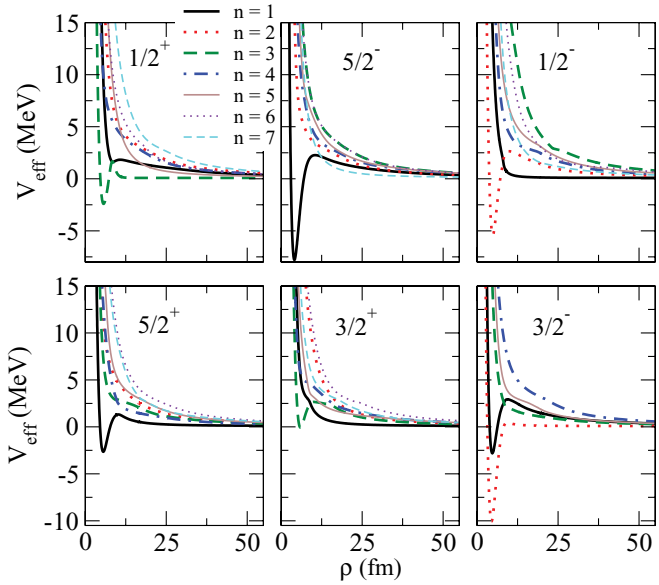

FIG. 3. (Color online) Real parts of the seven lowest adiabatic potentials as functions of the hyper-radius ρ for the $1/2^+$, $5/2^-$, $1/2^-$, $5/2^+$, $3/2^+$, and $3/2^-$ low-lying resonances in ^{9}Be.

the deepest potential for the $1/2^+$ resonance. In this case, the Q_{33} term is included, since this term is responsible for the potential barrier that permits holding the resonance (see Ref. [32] for details). The imaginary parts of the potentials are small, oscillate, and go to zero for large values of ρ. They are mostly related to the widths.

In Fig. 3, we observe that, at small distances, the lowest potentials have a pronounced well followed by a potential barrier that are responsible for the bound states and the resonances. We have two attractive potentials for angular momentum and parity $J^\pi = 3/2^-$; the deepest one supports the ground state (bound), while the other one supports the higher resonance. For other J^π values, only the lowest potential exhibits an attractive region at small distances. All the other potentials are repulsive at all distances.

At large distances, the lowest potential in all the cases approaches the ^{8}Be(0^+) resonance energy of $\sim$0.1 MeV. Its angular structure corresponds to the two α particles, which populate the ^{8}Be(0^+) resonance, while the remaining neutron is far away and is described through the radial equation. These specific potentials are labeled as number $n = 3$ in $1/2^+$, as $n = 7$ in $5/2^-$, as $n = 1$ in $1/2^-, 5/2^+$, and $3/2^+$, and as $n = 2$ in $3/2^-$. Then, they characterize a decay mechanism where the neutron first is emitted, and this two-body α-α resonance is populated and subsequently decays.

The complex scaling of the hyper-radius leads to a Hamiltonian with complex solutions, which vanish exponentially at large distances precisely as ordinary bound-state wave functions. The real and imaginary parts of the complex three-body energy are, respectively, the resonance energy E_R and $-\Gamma_R/2$, where Γ_R is the width of the resonance. The computed results are collected in Table I together with the known experimental values [33]. The three-body strength is adjusted to give the correct energy position for all J^π except for $3/2^-$, where we choose the same values for both bound state and resonance as in Ref. [34].

The energies are given relative to the α-α-n breakdown threshold, at 1.57 MeV above the ground state. We have found one bound state, which corresponds to the ^{9}Be ground state, and six resonances below 6 MeV of excitation energy. The ground state has $J^\pi = 3/2^-$, and the resonances have $1/2^\pm$, $3/2^\pm$, and $5/2^\pm$. Those states are most likely to contribute to processes, which bridge the $A = 5, 8$ instability gaps in nuclear synthesis in suitable astrophysical environments [35]. We keep the range of the three-body potential at $b = 5.0$ fm for all J^π, while adjusting the strength to place the resonance energies (and bound state) at the desired measured position. Thus, we did not attempt to reproduce the widths.

TABLE I. Calculated and measured energies E_R (in MeV) and widths Γ_R (in MeV) of the ^{9}Be resonances for different J^π. The experimental values (labeled exp) are from Ref. [33], and the calculated results (labeled th) are obtained with the three-body interaction parameter S (in MeV) (the range is taken $b = 5$ fm in all the cases). The energies are measured from the $\alpha\alpha n$ threshold.

J^π	$E_{R,\mathrm{exp}}$	$\Gamma_{R,\mathrm{exp}}$	$E_{R,\mathrm{th}}$	$\Gamma_{R,\mathrm{th}}$	S
$3/2^-$	-1.574	0.0	-1.60	0.0	2.5
$1/2^+$	0.110 ± 0.020	0.214 ± 0.005	0.11	$\simeq$0.1	–
$5/2^-$	0.855 ± 0.013	$(7.8 \pm 1.3) \times 10^{-4}$	0.86	7.0×10^{-4}	3.7
$1/2^-$	1.21 ± 0.12	1.10 ± 0.12	1.25	0.65	2.0
$5/2^+$	1.475 ± 0.009	0.282 ± 0.011	1.46	0.34	0.7
$3/2^+$	3.130 ± 0.025	0.743 ± 0.055	3.12	1.74	1.0
$3/2^-$	4.02 ± 0.01	1.33 ± 0.36	2.65	0.93	2.5

Several features are interesting in Table I. First, the three-body potentials have very moderate strengths, which were found to reproduce the real part of the measured energies. This is fine-tuning and strongly indicates that the dominating structures, in fact, really are three-body clusters. Then, it is significant that all widths, except for $1/2^\pm$ and the very narrow $5/2^-$ state, are larger than the corresponding measured values. This is consistent with a many-body configuration at small distances, which would decrease the branching ratio of decay into the investigated three-body cluster structure. A possible quantification of this deviation is in terms of preformation factors, which express that only part of the complete wave function describes the three-body cluster. Again, the deviation amounts to about factors of 2 in agreement with only smaller contributions from a many-body structure. A smaller range compensated by a slightly larger strength to leave the energy untouched would decrease the width toward the measured values.

However, the $3/2^-$ state is another exception in Table I. The computed value of width is smaller than the experimental table value. The computed energy is also below measurements by about 1.4 MeV. An attempt to increase the computed energy by this amount with the use of a repulsive three-body potential of range 5 fm immediately causes the resonance to disappear into the continuum, which corresponds to an energy above the barrier. This shows that the width in the model becomes very large very quickly and exceeds the experimental table value. Either the model is missing an important ingredient for this state, or its width should be substantially larger.

The $1/2^\pm$ states are an apparent exception in Table I, where the experimental widths are larger than the calculated values. For $1/2^+$, this discrepancy has caused a good deal of trouble. In a recent investigation [32], this conundrum was explained as a genuine three-body effect, where the resonance structure changes from dominantly ^{5}He plus an α particle at small distances to ^{8}Be plus a neutron at large distances. The large measured width is, in fact, obtained from an assumption of two-body character and sequential decay in the R-matrix analysis of the photodissociation cross section [23]. It is remarkable that a much smaller width consistent with Ref. [32] already was obtained many years ago [8]. The large experimental width of $1/2^-$ should be reevaluated, since we suspect that the R-matrix parametrization and the sequential decay channel are used too strongly in the extraction from the data analysis. This was argued for $1/2^+$ in Ref. [32].

B. Partial waves

The different two-body components of the three-body system are constrained by the total angular momentum and parity of each state. For example, in the first Jacobi (see Fig. 2), the two α particles must couple to an even orbital

angular momentum ℓ_x. A neutron with even (odd) angular momentum ℓ_y will give a positive-parity (negative-parity) state. The orbital angular momentum ℓ_y couples to the spin of the neutron to the angular momentum j_y. In the second Jacobi set, ℓ_x can be either even or odd and couples to the spin of the neutron to the angular momentum j_x.

We choose our partial-wave components by taking these selection rules into account. In the present case, convergence is achieved with a number of partial waves between 10 and 30, which depend on the resonance. The accuracy is optimized by choosing a large value for the hypermomentum K for the large contributions. Unfortunately, the higher the value of $K_{\max}$, the larger the total number of basis states. Therefore, $K_{\max}$ must be chosen carefully for each partial wave, which tries to achieve accuracy while keeping the number of basis elements as small as possible.

Tables II and III show, for the first and second Jacobi sets, the contributions W to the total J^π wave functions from those components that contribute more than 1%. These contributions are well defined for the complex-rotated resonance wave function, since it behaves asymptotically like a bound state.

TABLE II. Components included for each J^π state of ^{9}Be relative to the first Jacobi set (see Fig. 2). q labels the set of quantum numbers ℓ_x, ℓ_y, and j_y (coupling between ℓ_y and the spin of the neutron), which are the angular momenta relative to x and y Jacobi coordinates. $K_{\max}$ is the maximum value of the hypermomentum, and W gives the probability in percentage for finding these components in the resonance. Only the components contribute more than 1% are shown.

J^π	q	ℓ_x	ℓ_y	j_y	$K_{\max}$	$W(\%)$
$\frac{1}{2}^+$	1	0	0	$\frac{1}{2}$	150	100
$\frac{5}{2}^-$	1	0	3	$\frac{5}{2}$	95	1
	2	2	1	$\frac{1}{2}$	50	11
	3	2	1	$\frac{3}{2}$	75	83
	4	2	3	$\frac{7}{2}$	50	2
$\frac{1}{2}^-$	1	0	1	$\frac{1}{2}$	220	42
	2	2	1	$\frac{3}{2}$	180	55
	3	4	3	$\frac{7}{2}$	150	2
$\frac{5}{2}^+$	1	0	2	$\frac{5}{2}$	125	52
	2	2	0	$\frac{1}{2}$	120	27
	3	2	2	$\frac{5}{2}$	100	12
	4	2	4	$\frac{9}{2}$	60	4
$\frac{3}{2}^+$	1	0	2	$\frac{3}{2}$	175	10
	2	2	0	$\frac{1}{2}$	155	73
	3	2	2	$\frac{3}{2}$	85	4
	4	2	2	$\frac{5}{2}$	35	9
	5	4	2	$\frac{5}{2}$	35	3
$\frac{3}{2}^-$	1	0	1	$\frac{3}{2}$	170	3
	2	2	1	$\frac{1}{2}$	70	51
	3	2	1	$\frac{3}{2}$	80	41
	4	2	3	$\frac{7}{2}$	40	3

TABLE III. The same as Table II for the second Jacobi set (see Fig. 2). The angular momentum j_x results from the coupling between ℓ_x and the spin of the neutron.

J^π	q	ℓ_x	j_x	ℓ_y	$K_{\max}$	$W(\%)$
$\frac{1}{2}^+$	1	0	$\frac{1}{2}$	0	150	50
	3	1	$\frac{3}{2}$	1	89	50
$\frac{5}{2}^-$	1	1	$\frac{1}{2}$	2	50	11
	2	1	$\frac{3}{2}$	2	70	73
	3	2	$\frac{5}{2}$	1	30	9
	4	2	$\frac{5}{2}$	3	65	1
$\frac{1}{2}^-$	1	0	$\frac{1}{2}$	1	150	4
	2	1	$\frac{1}{2}$	0	200	35
	3	1	$\frac{3}{2}$	2	200	50
	4	2	$\frac{3}{2}$	1	150	6
	5	2	$\frac{5}{2}$	3	120	1
$\frac{5}{2}^+$	1	0	$\frac{1}{2}$	2	95	1
	2	1	$\frac{1}{2}$	3	95	5
	3	1	$\frac{3}{2}$	1	125	50
	4	1	$\frac{3}{2}$	3	95	5
	5	2	$\frac{3}{2}$	2	95	1
	6	2	$\frac{5}{2}$	0	95	25
$\frac{3}{2}^+$	1	0	$\frac{1}{2}$	2	99	27
	2	1	$\frac{1}{2}$	1	99	21
	3	1	$\frac{3}{2}$	1	55	12
	4	1	$\frac{3}{2}$	3	99	21
	5	2	$\frac{3}{2}$	0	25	6
	6	2	$\frac{5}{2}$	2	35	3
$\frac{3}{2}^-$	1	0	$\frac{1}{2}$	1	60	1
	2	1	$\frac{1}{2}$	2	50	45
	3	1	$\frac{3}{2}$	0	95	3
	4	1	$\frac{3}{2}$	2	90	34
	5	2	$\frac{3}{2}$	1	50	6
	6	2	$\frac{5}{2}$	1	50	5

The maximum value of the hypermomentum K is also given for each component. The computed values of W are given in the last column of the tables. The wave functions are located at relatively small distances, and the contribution from the different components (obtained after integration of the square of the wave function over all the hyperangular variables), therefore, contains information mainly about these bulk structures. The decay properties are contained in the large-distance tails, whose partial-wave content can be entirely different, as discussed in detail in Sec. IV.

The lowest resonance $J^\pi = \frac{1}{2}^+$ is located only 18 keV above the two-body ^{8}Be narrow ground-state resonance at 918 keV. In the first Jacobi coordinates, this state is entirely described as s waves between the α particles and, therefore, between their center of mass and the neutron. The interesting

structure is seen in the two other identical Jacobi coordinates where the structure changes abruptly from α neutron $p_{3/2}$ to $s_{1/2}$ configurations at around 10 fm, see Ref. [32]. The bulk part of the resonance structure found at small distances then roughly amounts to equal parts in each of these partial waves.

The next resonance with $J^\pi = \frac{5}{2}^-$ is very narrow because of the large barrier in the dominating partial wave of $(\ell_x, \ell_y) = (2, 1)$ in the first Jacobi and $(1, 2)$ in the second set of Jacobi coordinates. This can be described as ^{8}Be(2^+) or ^{5}He$(p_{3/2})$, respectively, but it is, in fact, the same state in different coordinate systems. Therefore, it is not meaningful to distinguish between these configurations unless spatial distributions also are included in the distinction [28].

The $\frac{1}{2}^-$ resonance is a result of the ^{5}He p-wave attraction combined with orbital angular momentum coupling to 2 of the last α particle. Only the corresponding adiabatic potential is really attractive. This configuration translates to $(\ell_x, \ell_y) = (0, 1), (2, 1)$ in the first Jacobi coordinates where only even ℓ_x are allowed.

The $\frac{5}{2}^+$ resonance is dominated by a combination of ^{5}He$(p_{3/2})$ and ^{8}Be$(0^+, 2^+)$. Only one of the adiabatic potentials is really attractive and, in fact, not very deep. This state is important at moderate temperatures for photodissociation and three-body recombination from the continuum via $E1$ transitions [35].

The next resonance $\frac{3}{2}^+$ is higher. Its structure is similar to the $\frac{5}{2}^+$ state in the first Jacobi where $(\ell_x, \ell_y) = (0, 2), (2, 0)$ are roughly interchanged in the two states. In the second Jacobi system, the ^{5}He$(p_{3/2})$ structure also has a relevant, although not dominant, contribution.

The last resonance $\frac{3}{2}^-$ has $(\ell_x, \ell_y) = (2, 1)$ and $(1, 2)$ in the first and second Jacobi sets, respectively. This reflects a combination of the influence of the interactions related to the ^{5}He$(p_{3/2})$ and ^{8}Be(2^+) two-body resonances. The similarity to the $\frac{5}{2}^-$ state is striking, except for the larger width, which arises from a higher excitation energy.

IV. LONG-DISTANCE STRUCTURE

Resonances may be populated at small distances via β decay or some specific reactions, but the products after the resonance decay reflect the behavior at large distances. The short- and large-distance structures are related through the quantum-mechanical solution, and the configurations sometimes change dramatically with the hyper-radius. Therefore, this connection from small to large distances is crucial for the interpretation of the decay mechanism and the measured results. We will first show the dynamic evolution of each resonance configuration, and afterward will show the momentum distributions of the fragments as Dalitz plots with the full information.

A. Dynamic evolution

As mentioned in Sec. III A, at large distances, the lowest adiabatic potential, for all the resonances, approaches the ^{8}Be(0^+) resonance energy of $\sim$0.1 MeV. Its angular structure corresponds to the two α particles, which populate the ^{8}Be(0^+) resonance, while the remaining neutron is far away. In other words, for large values of ρ, the configuration of this potential in the first Jacobi set approaches $\ell_x = 0$, $j_y = J$, and ℓ_y has to be one of the $J \pm 1/2$ values to produce the correct parity.

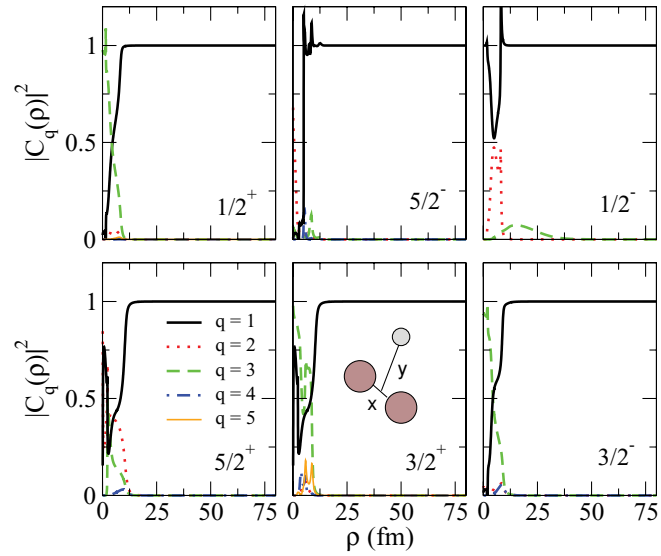

FIG. 4. (Color online) Contribution, as a function of ρ, of the different partial waves in the first Jacobi set (labeled with q as in Table II) to the adiabatic eigenfunction $\Phi_q(\rho, \Omega)$ related to the ground-state structure of ^{8}Be at large distance.

If this state is populated at large distances, where all couplings to other adiabatic potentials have vanished, the decay can be described as sequential via the ^{8}Be two-body ground state. Such a decay has a special role because it is favored by a very low energy with nonvanishing coupling to other potentials for all the resonances. Figures 4 and 5 show the partial-wave decomposition, as a function of the hyper-radius, for this adiabatic component. Not surprisingly, the dominant partial wave in the first set of Jacobi sets is the

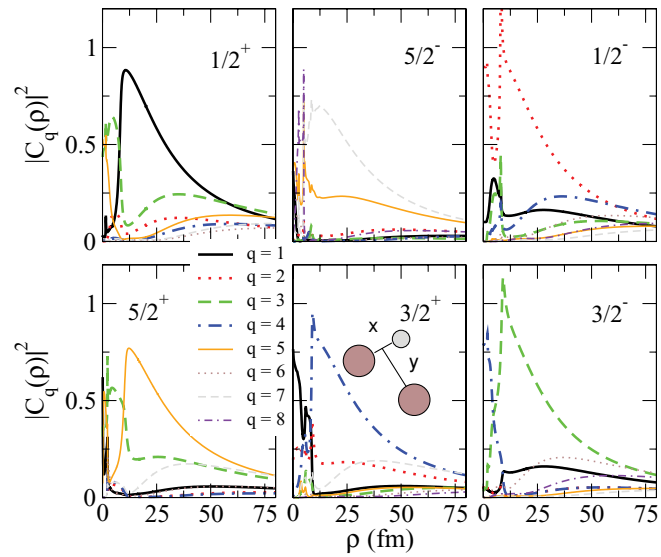

FIG. 5. (Color online) The same as in Fig. 4 but for the second Jacobi set. q labels the set of quantum numbers as in Table III.

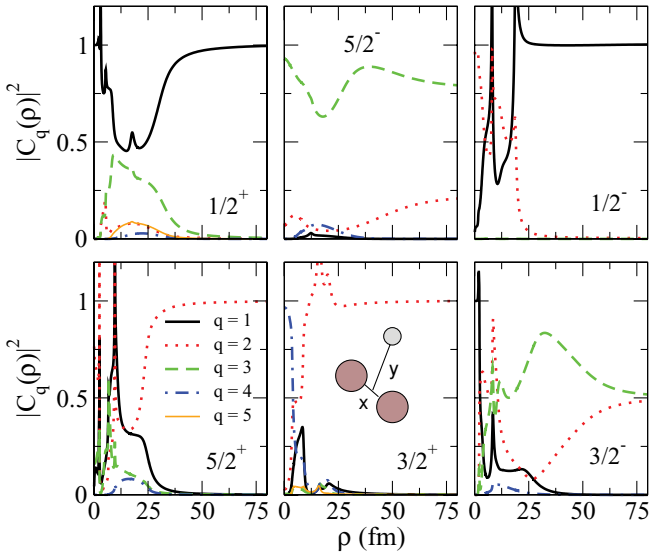

FIG. 6. (Color online) Contribution, as a function of ρ, of the different partial waves in the first Jacobi set (labeled with q as in Table II) to the dominant adiabatic eigenfunction $\Phi_q(\rho, \Omega)$ different from the one related to the ground-state structure of ^{8}Be at large distances.

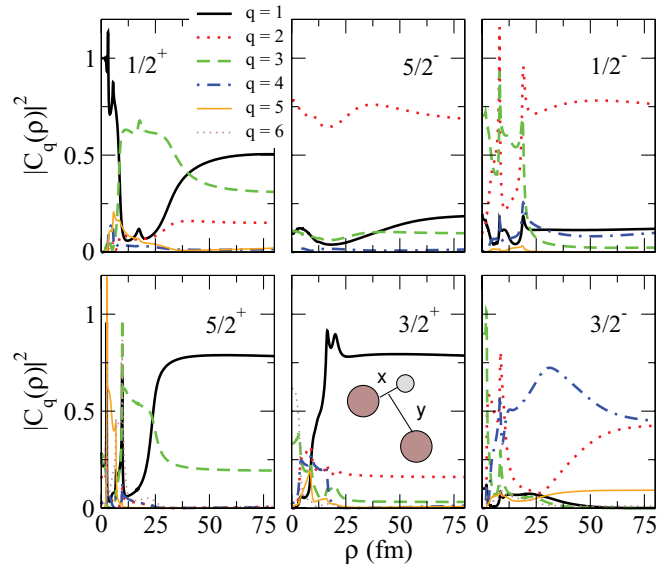

FIG. 7. (Color online) The same as in Fig. 6 but for the second Jacobi set. q labels the set of quantum numbers in each component as in Table III.

^{8}Be(0^+) structure for ρ values beyond about 10 fm, see Fig. 4. The same simple structure does not appear in the second Jacobi coordinates, as seen in Fig. 5. At short distances, around 20 fm, one of the components gives most of the contribution, but this structure is not maintained at large distances, where we observe a very fragmented partial-wave decomposition. The reason is, of course, that the transformation of the $\ell_x = 0$ state in the first Jacobi set into the second one results in contributions from many different angular momentum components.

The sequential decay via the ^{8}Be ground state leads to very simple momentum distributions derived from the two-body character, where energy and momentum conservation fully determine the final state. The remaining part of the decay proceeds through other adiabatic components. In Figs. 6 and 7, we show the partial-wave decomposition as a function of hyper-radius for the most contributing of these other components.

Each of the J^π states presents its own features. In all cases, the variation from small to large distances is substantial and sometimes dramatic. The structures always converge at large distances. In the first Jacobi (Fig. 6), after convergence, one of the partial waves absorbs almost all the contribution for the resonance of $1/2^+$, $1/2^-$, $5/2^+$, and $3/2^+$. The corresponding partial waves have $\ell_x = 0$, 0, 2, and 2, respectively. They are, therefore, related to 0^+ and 2^+ states in ^{8}Be. In the $5/2^-$ resonance, there are two partial waves, which contribute significantly, but one of them dominates with $\ell_x = 2$ and, thus, is related to a ^{8}Be(2^+) structure [28]. In contrast, the $3/2^-$ resonance has two components with $\ell_x = 2$ that are equally important at large values of ρ.

In Fig. 7, we show the partial-wave decomposition for these resonances in the second Jacobi system. The $1/2^+$ state presents a mixture of three components, which contribute significantly at large distances. This is somewhat analogous to the transform of the ^{8}Be ground state with many partial waves at large distances. Here, we only find three, which, therefore, also emphasizes that even with the same quantum numbers (all s waves), the structure can be very different. The $5/2^-$ and $1/2^-$ states reveal structures where each converges to quantum numbers identical to those of ^{5}He($p_{3/2}$) and ^{5}He($p_{1/2}$), respectively. Again, this does not imply that these are the decay channels, only the quantum numbers are the same. In $5/2^+$ and $3/2^+$, the dominant components at large distances have $\ell_x = 0$ as for the ^{8}Be ground state, but the behavior differs very much from those of Fig. 5. The last state of $3/2^-$ presents two roughly equal contributions both with $(\ell_x, \ell_y) = (1, 2)$ very much like in the first Jacobi system. It is like ^{8}Be(0^+) is replaced by the ^{5}He(p state).

B. Momentum distributions

The decay mechanisms depend on the resonance properties, and they are conventionally called either sequential via a given two-body structure or direct decay to the continuum or perhaps a mixture of these possibilities. The process is sequential when the measured kinematics reveals that one particle is first emitted and, subsequently, the remaining structure decays into two fragments independent of the emission of the first particle. Combinations of such decay channels form the basis for the R-matrix analyses of experimental data [36]. This formulation becomes dubious when the intermediate two-body structure falls apart on the same time scale as the first emission. The process is then better described as a genuine three-body decay. This does not prevent analyses in terms of several two-body decay channels. The two different formulations may still be completely identical provided the two different sets of basis functions span the same space. The two formulations merely differ in the choice of basis [37].

TABLE IV. ^{9}Be resonance excitation energies, energies above the $\alpha\alpha n$ threshold, and, for each resonance, estimated amount of computed and observed sequential decay via ^{8}Be(0^{+}).

J^{π}	$E_{\alpha\alpha n}$ (MeV)	$E_{\rm res}$ (MeV)	Theo. (%)	Exp. (%) [27]	Exp. (%) [39,40]	Exp. (%) [41]
$\frac{1}{2}^{+}$	1.68	0.11	100			100
$\frac{5}{2}^{-}$	2.43	0.86	3	6 ± 1	7 ± 1	
$\frac{1}{2}^{-}$	2.82	1.25	90	32 ± 15	100	
$\frac{5}{2}^{+}$	3.03	1.46	53	46 ± 20	87 ± 13	
$\frac{3}{2}^{+}$	4.69	3.12	1	16 ± 2		
$\frac{3}{2}^{-}$	4.22	2.65	29			

The present case is in one way rather simple, since all the resonances can decay sequentially via ^{8}Be(0^{+}), which is a long-lived stable structure that survives a long time after emission of the neutron. Thus, the sequential decay mechanism through this state is not controversial and easily separated kinematically in experiments. One of the adiabatic components is related to the $^{8}\mathrm{Be} + n$ structure and approaches the energy of the ^{8}Be(0^{+}) resonance. This component describes the sequential decay contribution through this channel. Extension of this picture to sequential decays through ^{8}Be(2^{+}) or ^{5}He($p_{3/2}$) is an invitation for difficulties, since these channels are broad (short-lived) resonance structures, not easily separated from the background continuum, and, furthermore, not even orthogonal contributions. This is more reasonably described as a direct decay.

The technique involved is described in Ref. [38] where the large-distance asymptotic behavior of the radial wave functions are shown to give the branching ratio for such sequential decay. We have calculated this fraction of decay for each of the ^{9}Be resonances. The result is given in Table IV. The decays of $\frac{1}{2}^{\pm}$ are found to be predominantly sequential. In $\frac{5}{2}^{+}$, both mechanisms are comparable, whereas the direct decays dominate for the other three resonances. The comparison to measured branching ratios is rather favorable in view of the uncertainties for broad resonances and the different methods of extraction.

The uncertainties are especially emphasized by considering the $\frac{1}{2}^{-}$ state, which often is quoted as predominantly decaying through the ^{8}Be ground state [18,19] in agreement with our result. This is intuitively appealing, since the alternative channels of ^{8}Be(2^{+}) and ^{5}He($p_{1/2}$) are rather high lying. Also, more recently, contributions through such channels are extracted from experimental analysis [25,27], although given with reservations and uncertainties. Furthermore, the β feeding, the width, and the decay channel are linked together for broad resonances in data analysis [21]. We conjecture that the width should be smaller than the measured value in Table I, and the predominant decay channel is through the ground state of ^{8}Be.

For the sequential channels, the resulting momentum distributions are easily found, since the first emission immediately provides the energy of the particle in the three-body center-of-mass system. The following decay is again given by one energy in the center-of-mass system of the remaining two particles.

The momentum distributions for direct decays into the continuum can now be found by excluding the sequential contribution, that is, the part of the wave function, which resides in the ^{8}Be ground state at large distances. Again, we have to calculate, as accurately as possible, the large-distance asymptotics of the wave function. The technique, described in Refs. [42,43], is based on finding the Zeldovic regularized Fourier transform of the coordinate-state wave resonance function. The result is directly comparable to measured distributions. It is worth emphasizing again that the only link from the asymptotic measurable distribution to the small-distance structure is via theoretical models [28].

We compute the distributions by Monte Carlo simulation. First, we randomly generate a large number of events, each of them, which consists of three four momenta relative to our three decaying fragments. The sum of their center-of-mass energies must equal the resonance energy. The weight of each set of momenta is the absolute-squared wave function at large distances. The resulting energy distributions are shown in Figs. 8 and 9 for α particles and neutrons, respectively. We give the energies in units of their maximum values for each case (i.e., $5/9E_{\rm res}$ for the α's and $8/9E_{\rm res}$ for the neutrons).

The distributions all necessarily have peaks, since they start with zero and return again to zero at maximum energy. However, they can have more than one peak, and each of them has an individual position and width. The $5/2^{-}$ and $3/2^{-}$ resonances are smooth with one peak for both neutrons and α particles. In both cases, the neutron energies peak below and the α particle above half of their respective maximum values. This means a tendency to emit α particles in essentially opposite directions, while leaving the remaining neutron in the middle with relatively little energy. This is only a tendency, and the full distributions require detailed computations. Still, it is indicative for this part of the process.

For the $1/2^{-}$ decay, the α particle shows up with a broad distribution on the low-energy side, whereas the neutron appears on the high-energy side. This resembles the sequential decay through the ^{8}Be ground state where α particles end up with only little energy. However, the present decay has to proceed through an orthogonal adiabatic potential, which reveals itself by the low-energy node in the distribution of the neutron energy.

The $3/2^{+}$ and $5/2^{+}$ resonances both produce neutrons and α's with tendencies to be on high- and low-energy sides,

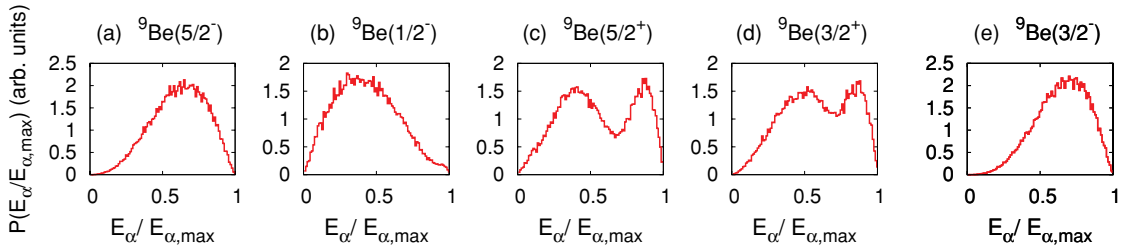

FIG. 8. (Color online) α-particle energy distributions for (a) the $5/2^-$ resonance of ^{9}Be at 2.43 MeV of excitation energy (or 0.86 MeV above the $\alpha\alpha n$ threshold), (b) the $1/2^-$ resonance of ^{9}Be at 2.82 MeV of excitation energy (or 1.25 MeV above the $\alpha\alpha n$ threshold), (c) the $5/2^+$ resonance of ^{9}Be at 3.03 MeV of excitation energy (or 1.46 MeV above the $\alpha\alpha n$ threshold), (d) the $3/2^+$ resonance of ^{9}Be at 4.69 MeV of excitation energy (or 3.12 MeV above the $\alpha\alpha n$ threshold), and (e) the $3/2^-$ resonance of ^{9}Be at 4.22 MeV of excitation energy (or 2.65 MeV above the $\alpha\alpha n$ threshold). The energies are divided by the maximum possible (i.e., $5/9E_{\rm res}$). The sequential decay via ^{8}Be(0^+) has been removed in all cases.

respectively, such as for the $5/2^-$ and $3/2^-$ resonances. However, in the positive-parity cases, additional peaks appear in both distributions, again a signal of an excited state. These cases are otherwise not very similar, and the distributions are very broad, each extending across from the high- to the low-energy side and vice versa.

These distributions can be suggestive and deceiving. The momenta are distributed among all three particles, which is the reason for the continuous distributions in the first place. However, this also means that a kinematically complete description for a given conserved total resonance energy requires energies of two particles at the same time. This information is contained in the two-dimensional energy correlations known as Dalitz plots, which were introduced by Dalitz in (1953) to study decays of K mesons [44]. These correlation diagrams provide an excellent tool for studying the dynamics of three-body decays. The technique has recently been picked up and has been applied in studies of nuclear fragmentation processes [45]. In simple two-body decays, the angular distribution of the emitted particles carries the signature of decaying angular momentum and parity. The Dalitz plots are generalizations to three-body decays, and it is natural to use the plots in attempts of experimentally assigning spin and parity to the decaying resonances [37].

To establish the connection to measured distributions, we computed Dalitz plots for α particles and neutrons after the decay of ^{9}Be resonances. We use the same Monte Carlo technique as for the individual particle energy distributions. To facilitate comparison with the experimental results from Ref. [27], we plot the α-n relative energies on the x and y axes, that is,

$$E_{\alpha-n} = \frac{|\boldsymbol{p}_{\alpha-n}|^2}{2\mu_{\alpha n}}, \quad \boldsymbol{p}_{\alpha-n} = \frac{\mu_{\alpha n}}{m_\alpha}\boldsymbol{p}_\alpha - \frac{\mu_{\alpha n}}{m_n}\boldsymbol{p}_n, \tag{11}$$

where $\boldsymbol{p}_{\alpha-n}$ is the relative momentum. The results are shown in Fig. 10. We first observe that all the distributions are symmetric with respect to interchange of the axes. This is necessary and reflects that the wave functions are symmetric for the identical bosonic α particles.

The graphs that correspond to $\frac{5}{2}^-$ and $\frac{3}{2}^-$ are very similar to each other. None of them exhibits any points or regions of zero probability, except on the confining envelope defined by energy conservation. This means that symmetry, angular momentum, and parity of these structures $(\ell_x, \ell_y) = (1, 2), (2, 1)$ (Tables II and III) allow emission in all directions and with all energy partitions.

The probability increases toward higher α energies, which corresponds to smaller relative energies, since the neutron is much lighter than the α particle. This is caused by the Coulomb repulsion and the tendency to choose a decay path where the neutron is left in the middle as observed in the one-dimensional energy distributions, see Figs. 8 and 9. Distributions for both states compare well with the experimental plots from Ref. [27]. Moreover, the $\frac{5}{2}^-$ distribution is very similar to the measured ones published in Ref. [26] and is investigated theoretically in detail in Ref. [28].

The distributions for $\frac{1}{2}^-$, $\frac{5}{2}^+$, and $\frac{3}{2}^+$ exhibit much more structure, and all have zero probability regions as reflected in the nodes or minima of the one-dimensional distributions.

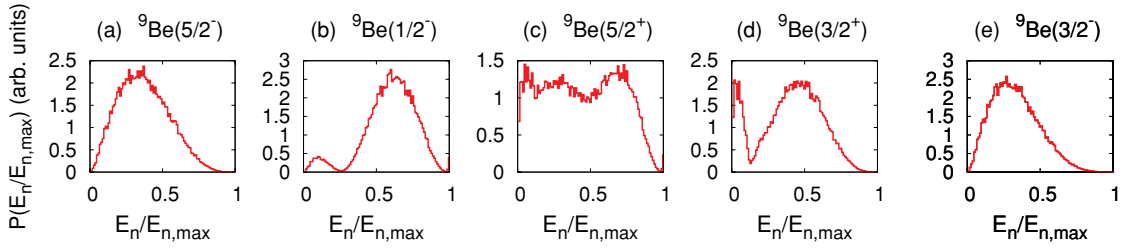

FIG. 9. (Color online) The same as Fig. 8 for the neutron-energy distributions. The energies are divided by the maximum possible !l (i.e., $8/9E_{\rm res}$).

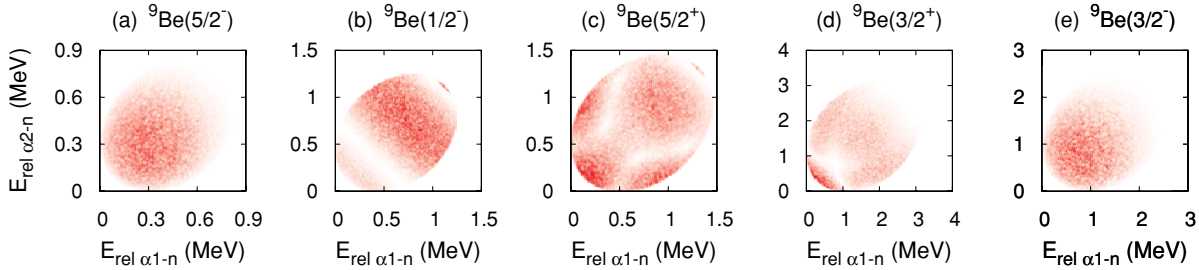

FIG. 10. (Color online) Dalitz plots for (a) the $5/2^-$ resonance of ^{9}Be at 2.43 MeV of excitation energy (or 0.86 MeV above the $\alpha\alpha n$ threshold), (b) the $1/2^-$ resonance of ^{9}Be at 2.82 MeV of excitation energy (or 1.25 MeV above the $\alpha\alpha n$ threshold), (c) the $5/2^+$ resonance of ^{9}Be at 3.03 MeV of excitation energy (or 1.46 MeV above the $\alpha\alpha n$ threshold), (d) the $3/2^+$ resonance of ^{9}Be at 4.69 MeV of excitation energy (or 3.12 MeV above the $\alpha\alpha n$ threshold), and (e) the $3/2^-$ resonance of ^{9}Be at 5.59 MeV of excitation energy (or 4.02 MeV above the $\alpha\alpha n$ threshold). On the axis, we plot the α-n relative energy in MeV. The sequential decay via ^{8}Be(0^+) has been removed in all cases.

For $\frac{1}{2}^-$, we find a striking similarity with the measured distribution in Ref. [27] at the excitation energy window at 2.8 MeV. The very low probability bands at lower and higher relative energies are found in both places. The different projections on the neutron-energy axis in Fig. 9 resulted in a node at small neutron energy, presumably, which corresponds to a cut along the low-energy small probability region in Fig. 10.

For both $\frac{5}{2}^+$ and $\frac{3}{2}^+$, the computed distributions have lots of structure, whereas the measurements show more smooth distributions without much resemblance to calculations. The explanation for these discrepancies is still to be found.

V. SUMMARY AND CONCLUSIONS

The hyperspherical adiabatic expansion method, combined with complex scaling, is used to compute the energies and widths of ^{9}Be low-lying resonances. We describe them as three-cluster resonances ($\alpha\alpha n$). Realistic short-range nuclear interactions, as well as Coulomb interactions, are included in the computations. To reach high accuracy, we use a large hyperharmonic basis for each angular eigenfunction, accurate large distances, outgoing waves of radial wave functions and, if possible, the correct energy of the three-body resonance obtained by tuning the three-body potential.

We find one bound state ($\frac{3}{2}^-$) and six resonances below 6 MeV of excitation energy in agreement with experimental information. Spins and parities of the resonances are $\frac{1}{2}^\pm$, $\frac{3}{2}^\pm$, and $\frac{5}{2}^\pm$. The small-distance properties of the adiabatic potentials determine energies, while barriers at intermediate distances are crucial for the widths, and the large-distance structure of the resonances is decisive for the momentum partition between the three particles in the final state after decay.

The structure of the resonances is obtained as different combinations of angular momenta of the two-body subsystems. The configurations are determined by the interactions, which lead to observed low-lying resonances of the subsystems (i.e., 0^+, 2^+ for ^{8}Be and $p_{3/2}$ $p_{1/2}$ for ^{5}He). The detailed configurations of the three-body resonances are extracted, their energies fine-tuned via the three-body potential, and their widths computed.

We compute the possibly substantial dynamic evolution of the resonances as functions of hyper-radius. The large-distance asymptotic structures are via Fourier transformation directly related to the momentum distributions of the fragments after the three-body decay. We determine the fraction, which decays via the ground state of ^{8}Be in a sequential decay. The agreement with measurements is rather good in view of the uncertainties related to broad resonances and different theoretical and experimental definitions and methods.

The remaining part is described as direct decay to the three-body continuum. We present the computed momentum distributions of neutrons and α particles for each of the resonances. These observable distributions are results of the dynamic evolution and are open to experimental tests. We compare with the available data and find remarkable similarities except for the $5/2^+$, $3/2^+$ resonances, where the theory gives much more structure than found in the energy windows selected in the experiments.

ACKNOWLEDGMENTS

This work was partly supported by funds provided by DGI of MEC (Spain) under Contract No. FIS2008-01301 and the Spanish Consolider-Ingenio programme CPAN (Programme No. CSD2007-00042). R.A.R. acknowledges support by Ministerio de Ciencia e Innovación (Spain) under the Juan de la Cierva program. We have benefited from continuous discussions with H. O. U. Fynbo and K. Riisager.

[1] E. M. Henley and P. D. Kunz, Phys. Rev. **118**, 248 (1960).
[2] Y. C. Tang, F. C. Khanna, R. C. Herndon, and K. Wildermuth, Nucl. Phys. **35**, 421 (1962).
[3] J. Hiura and I. Shimodaya, Prog. Theor. Phys. **30**, 585 (1963).
[4] F. C. Barker, Nucl. Phys. **83**, 418 (1966).
[5] M. Bouten, M.-C. Bouten, H. Depuydt, and L. Schotsmans, Nucl. Phys. A **127**, 177 (1969).
[6] R. Grubman and T. Witten, Nucl. Phys. A **158**, 289 (1970).
[7] W. Zahn, Nucl. Phys. A **269**, 138 (1976).

[8] H. Furutani, H. Kanada, T. Kaneko, S. Nagata, H. Nishioka, S. Okabe, S. Saito, T. Sakuda, and M. Seya, Prog. Theor. Phys. Suppl. **68**, 193 (1980).
[9] A. C. Fonseca and M. T. Peña, Nucl. Phys. A **487**, 92 (1988).
[10] Y. Kanada-En'yo, H. Horiuchi, and A. Ono, Phys. Rev. C **52**, 628 (1995).
[11] K. Arai, Y. Ogawa, Y. Suzuki, and K. Varga, Phys. Rev. C **54**, 132 (1996).
[12] S. C. Pieper, K. Varga, and R. B. Wiringa, Phys. Rev. C **66**, 044310 (2002).
[13] L. V. Grigorenko, R. C. Johnson, I. G. Mukha, I. J. Thompson, and M. V. Zhukov, Eur. Phys. J. A **15**, 125 (2002).
[14] K. Arai, P. Descouvemont, D. Baye, and W. N. Catford, Phys. Rev. C **68**, 014310 (2003).
[15] C. Forssén, P. Navrátil, W. E. Ormand, and E. Caurier, Phys. Rev. C **71**, 044312 (2005).
[16] E. T. Ibraeva, M. A. Zhusupov, A. Y. Zaykin, and S. S. Sagindykov, Phys. At. Nucl. **72**, 1719 (2009).
[17] J. Mösner, G. Schmidt, and J. Schintlmeister, Nucl. Phys. A **64**, 169 (1965).
[18] P. R. Christensen and C. L. Cocke, Nucl. Phys. A **89**, 656 (1966).
[19] Y. S. Chen, T. A. Tombrello, and R. W. Kavanagh, Nucl. Phys. A **146**, 136 (1970).
[20] H. Jeremie, L. Lemay, M. Irshad, and G. Kennedy, Nucl. Phys. A **312**, 43 (1978).
[21] G. Nyman *et al.*, Nucl. Phys. A **510**, 189 (1990).
[22] O. V. Bochkarev, Y. O. Vasil'ev, A. A. Korsheninnikov, E. A. Kuz'min, I. G. Mukha, V. M. Pugach, L. V. Chulkov, and G. B. Yan'kov, Sov. J. Nucl. Phys. **52**, 964 (1990).
[23] K. Sumiyoshi, H. Utsunomiya, S. Goko, and T. Kajino, Nucl. Phys. A **709**, 467 (2002).
[24] B. R. Fulton *et al.*, Phys. Rev. C **70**, 047602 (2004).
[25] Y. Prezado *et al.*, Phys. Lett. B **618**, 43 (2005); M. J. G. Borge, Y. Prezado, O. Tengblad, H. O. U. Fynbo, K. Riisager, and B. Jonson, Phys. Scr., T **125**, 103 (2006).
[26] P. Papka *et al.*, Phys. Rev. C **75**, 045803 (2007).
[27] T. A. D. Brown *et al.*, Phys. Rev. C **76**, 054605 (2007).
[28] R. Álvarez-Rodríguez, H. O. U. Fynbo, A. S. Jensen, and E. Garrido, Phys. Rev. Lett. **100**, 192501 (2008).
[29] E. Nielsen, D. V. Fedorov, A. S. Jensen, and E. Garrido, Phys. Rep. **347**, 373 (2001).
[30] S. Ali and A. R. Bodmer, Nucl. Phys. **80**, 99 (1966).
[31] A. Cobis, D. V. Fedorov, and A. S. Jensen, Phys. Rev. Lett. **79**, 2411 (1997).
[32] E. Garrido, D. V. Fedorov, and A. S. Jensen, Phys. Lett. B **684**, 132 (2010).
[33] F. Ajzenberg-Selove, Nucl. Phys. A **490**, 1 (1988); [http://www.nndc.bnl.gov/chart/].
[34] R. Álvarez-Rodríguez, E. Garrido, A. S. Jensen, D. V. Fedorov, and H. O. U. Fynbo, Eur. Phys. J. A **31**, 303 (2007).
[35] R. de Diego, E. Garrido, D. V. Fedorov, and A. S. Jensen, Europhys. Lett. **90**, 52001 (2010).
[36] A. M. Lane and R. G. Thomas, Rev. Mod. Phys. **30**, 257 (1958).
[37] H. O. U. Fynbo, R. Álvarez-Rodríguez, A. S. Jensen, O. S. Kirsebom, D. V. Fedorov, and E. Garrido, Phys. Rev. C **79**, 054009 (2009).
[38] R. Álvarez-Rodríguez, A. S. Jensen, E. Garrido, D. V. Fedorov, and H. O. U. Fynbo, Phys. Rev. C **77**, 064305 (2008).
[39] C. Angulo *et al.*, Nucl. Phys. A **656**, 3 (1999).
[40] D. R. Tilley, J. H. Kelley, J. L. Godwin, D. J. Millener, J. E. Purcell, C. G. Sheu, and H. R. Weller, Nucl. Phys. A **745**, 155 (2004).
[41] O. Burda, P. von Neumann-Cosel, A. Richter, C. Forssén, and B. A. Brown, Phys. Rev. C **82**, 015808 (2010).
[42] D. V. Fedorov, H. O. U. Fynbo, E. Garrido, and A. S. Jensen, Few-Body Syst. **34**, 33 (2004).
[43] E. Garrido, D. V. Fedorov, A. S. Jensen, and H. O. U. Fynbo, Nucl. Phys. A **766**, 74 (2006).
[44] R. H. Dalitz, Philos. Mag. **44**, 1068 (1953).
[45] H. O. U. Fynbo *et al.*, Phys. Rev. Lett. **91**, 082502 (2003).